Science Advances
AAAS

advances.sciencemag.org/cgi/content/full/5/7/eaaw7935/DC1

Supplementary Materials for

Cryo-EM structure of TRPC5 at 2.8-Å resolution reveals unique and conserved structural elements essential for channel function

Jingjing Duan*, Jian Li*, Gui-Lan Chen*, Yan Ge, Jieyu Liu, Kechen Xie, Xiaogang Peng, Wei Zhou, Jianing Zhong, Yixing Zhang, Jie Xu, Changhu Xue, Bo Liang, Lan Zhu, Wei Liu, Cheng Zhang, Xiao-Li Tian, Jianbin Wang, David E. Clapham, Bo Zeng*, Zongli Li*, Jin Zhang*

*Corresponding author. Email: zhangxiaokong@hotmail.com (J.Z.); zongli_li@hms.harvard.edu (Z.L.); xyaze@163.com (B.Z.)

Published 24 July 2019, *Sci. Adv.* **5**, eaaw7935 (2019)
DOI: 10.1126/sciadv.aaw7935

This PDF file includes:

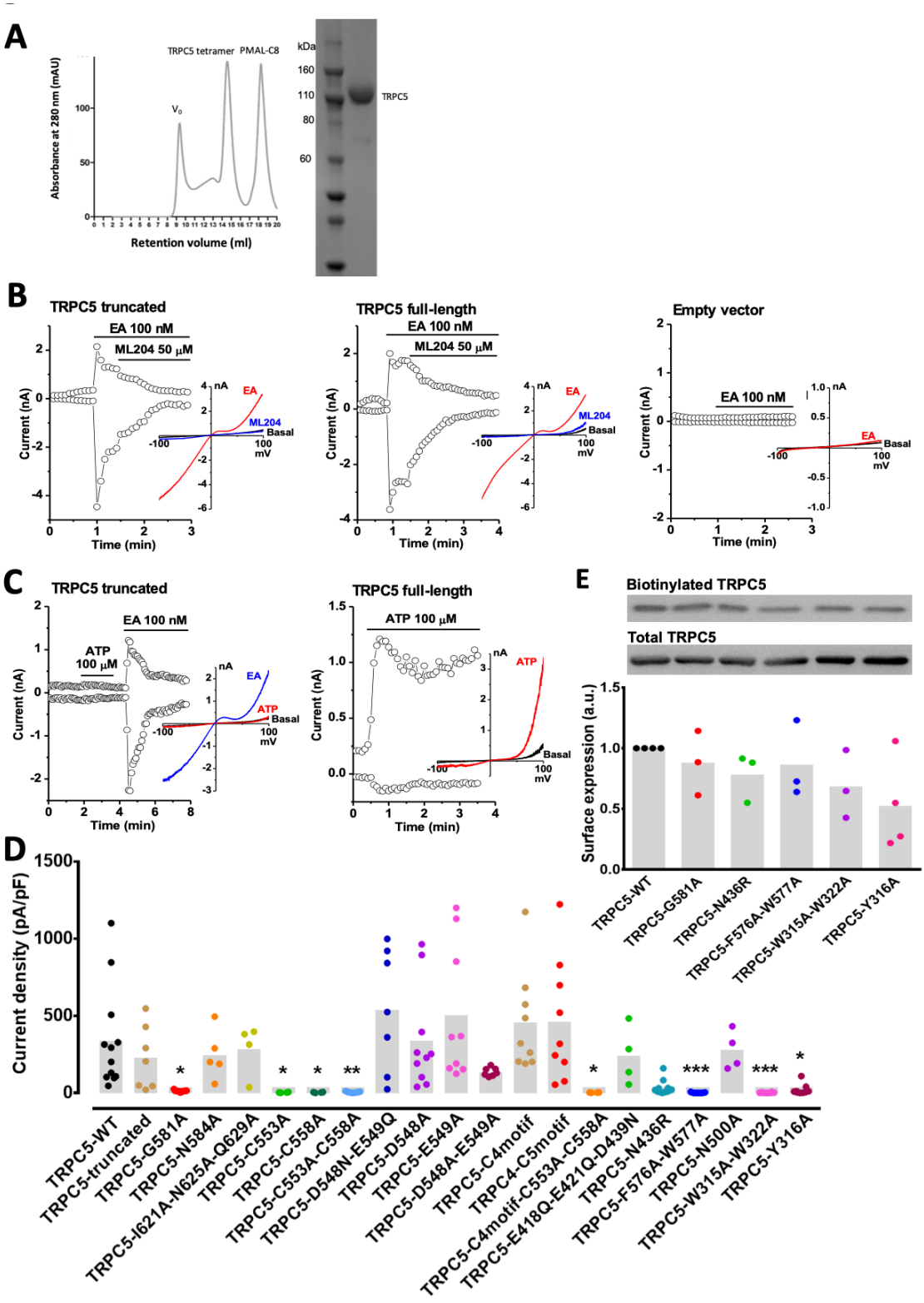

Fig. S1. Biochemical and functional characterization of the TRPC5 constructs. (A) Size exclusion chromatography of TRPC5 proteins. Void volume (V_0) and the peaks corresponding to tetrameric TRPC5 and PMAL-C8 are indicated. Protein samples of the indicated TRPC5 protein fraction were subjected to SDS-PAGE and Coomassie-blue staining. **(B)** Representative whole-cell patch clamp recordings and *I-V* relationships of truncated TRPC5,

full-length TRPC5, and empty vector-transfected HEK293 cells. The time course of currents measured at +80 and -80 mV and *I-V* relationships of the peak currents in different conditions are shown. Englerin A (EA) is an activator while ML204 is an inhibitor for TRPC4/5 channels. **(C)** Responses of the truncated and full-length TRPC5 constructs to G protein-mediated signaling. ATP is an agonist of G protein-coupled purinergic receptors $P2Y_2$ and $P2Y_{11}$, which are endogenously expressed in HEK293 cells. **(D)** Densities of peak currents at -80 mV evoked by 100-nM EA for TRPC5 constructs. **P*<0.05, ***P*<0.01, ****P*<0.001 *vs* TRPC5-WT, Dunn's multiple comparisons (*n*=4-12). **(E)** Quantification of cell surface expression of loss-of-function TRPC5 constructs (*n*=3-4). No statistical difference by ANOVA.

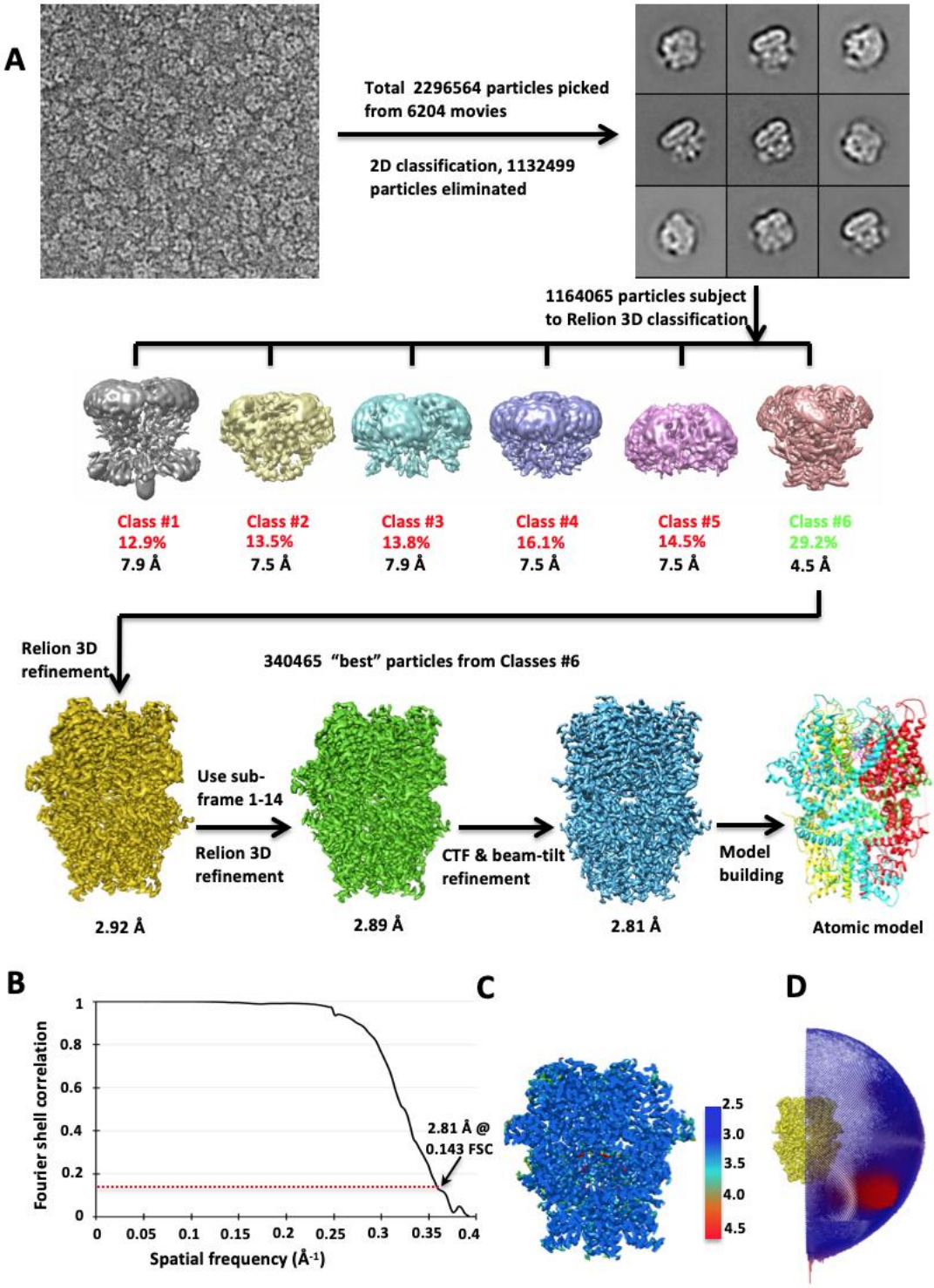

Fig. S2. Flow chart for TRPC5 cryo-EM data processing. (A) Representative image of the purified TRPC5 protein, 2D class averages of TRPC5 particles, side views of the 3D reconstructions from RELION 3D classification, and final 3D reconstructions from 3D auto-refinement. **(B)** Fourier shell correlation (FSC) curve for the 3D reconstruction (marked at overall 2.8 Å resolution). **(C)** Local resolution estimation from ResMap(*45*) and, **(D)** Euler

distribution plot of particles used in the final three-dimensional reconstruction. The length of the rod is proportional to the number of particles in that view, with regions in red denoting the views containing the highest number of particles.

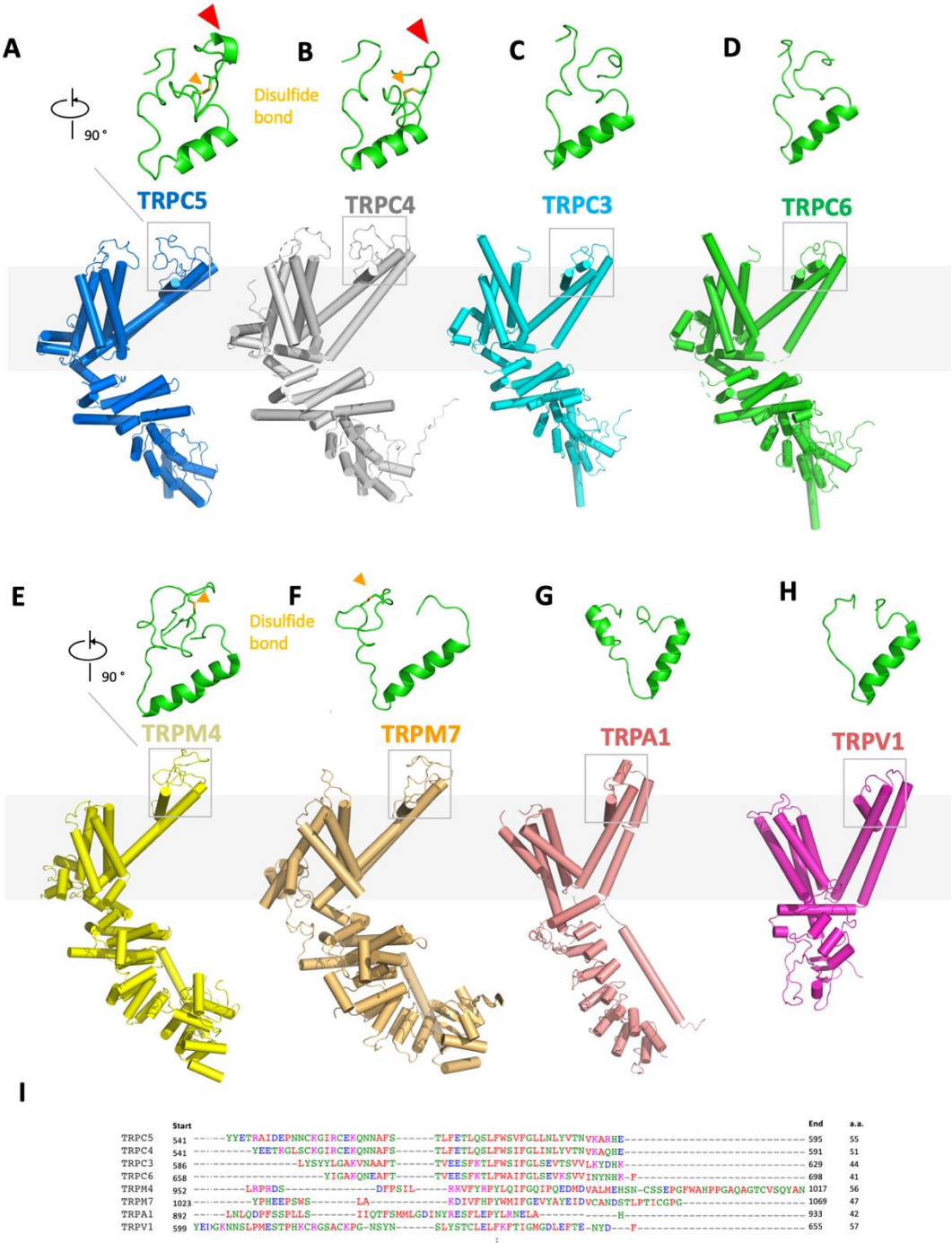

Fig. S3. Pore loop structures of known TRP channels. (A)-(H), Comparison of the pore loop in TRPC5 (**A.** PDB: 6AEI) with other known TRP channels, including TRPC4 (**B.** PDB: 5Z96), TRPC3 (**C.** PDB: 5ZBG), TRPC6 (**D.** PDB: 5YX9), TRPM4 (**E.** PDB: 6BWI), TRPM7 (**F.** PDB: 6BWD), TRPA1 (**G.** PDB: 3J9P) and TRPV1 (**H.** PDB: 5IRX). **(I)** Sequence alignment of the corresponding pore loop and linkers (shown as green helices and linkers in **A**-**H**).

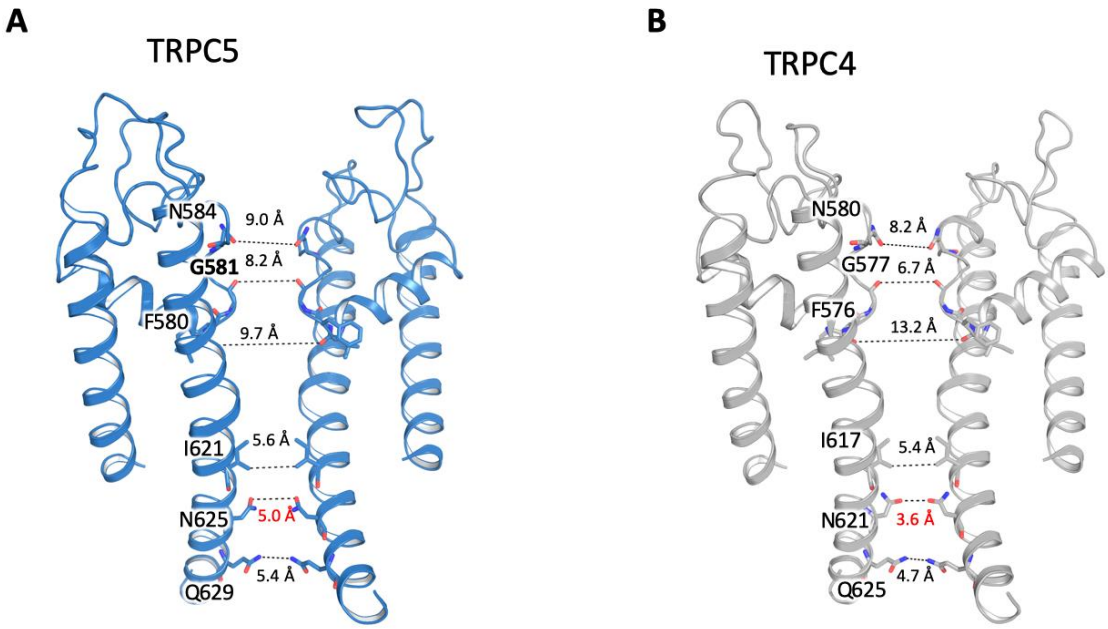

Fig. S4. Comparison of ion conducting pathways between TRPC5 and TRPC4.

Comparison of ion conduction pathways of **(A)** TRPC5, and **(B)** TRPC4 (PDB: 5Z96). Distances between specific side chains along the pore and the key residues are labeled.

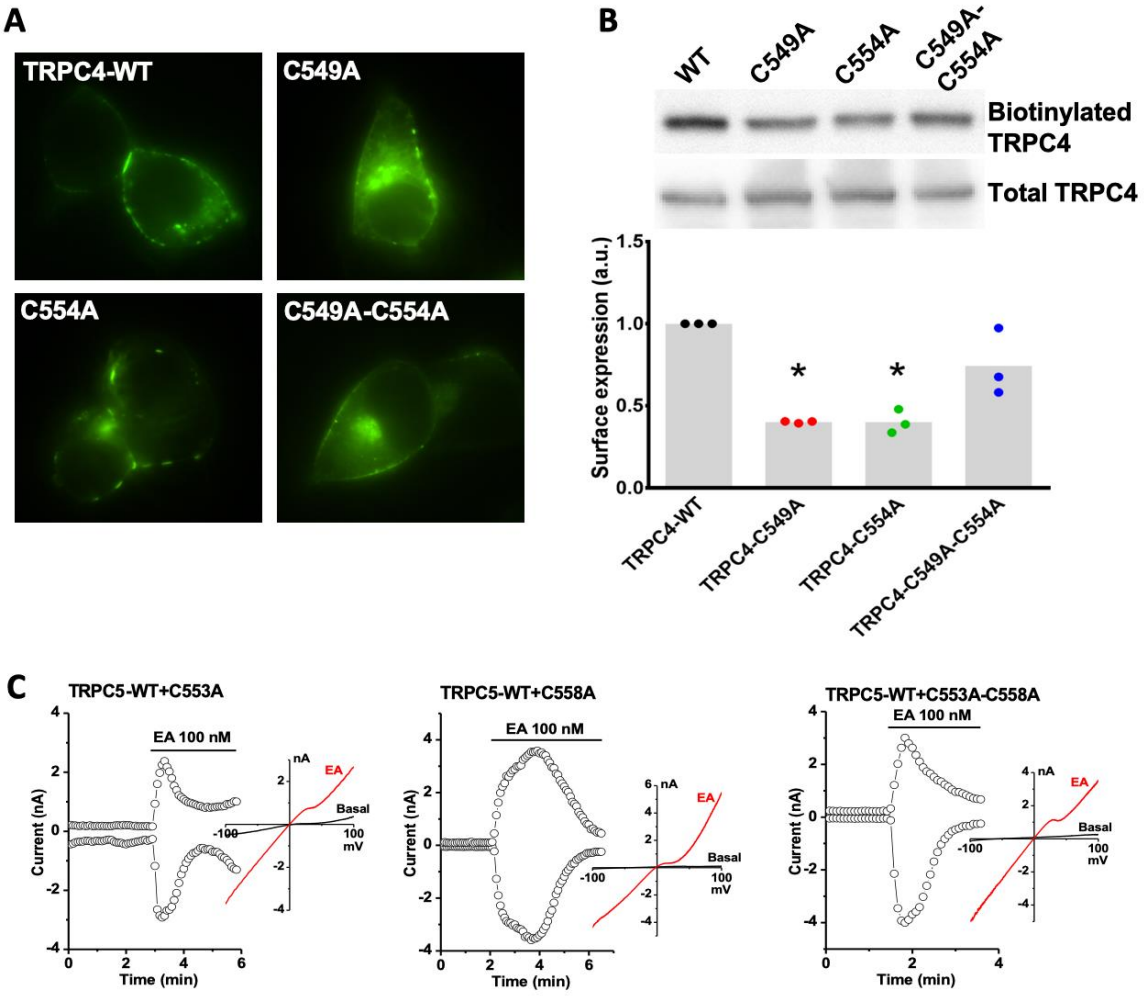

Fig. S5. Cell surface expression levels of TRPC4 cysteine mutants and function of TRPC5 cysteine mutants. (A) Localization of EYFP-tagged TRPC4 constructs in HEK293 cells. **(B)** Trafficking of TRPC4 to the plasma membrane was impaired by cysteine mutations. **P*<0.05 *vs* TRPC4-WT, Dunn's multiple comparison test (*n*=3). **(C)** Cysteine mutants do not suppress the activity of WT TRPC5. Whole-cell patch clamp recordings of WT TRPC5 cotransfected with different cysteine mutants in HEK293 cells. The time course of currents measured at +80 and -80 mV and *I-V* relationships of the peak currents in different conditions are shown.

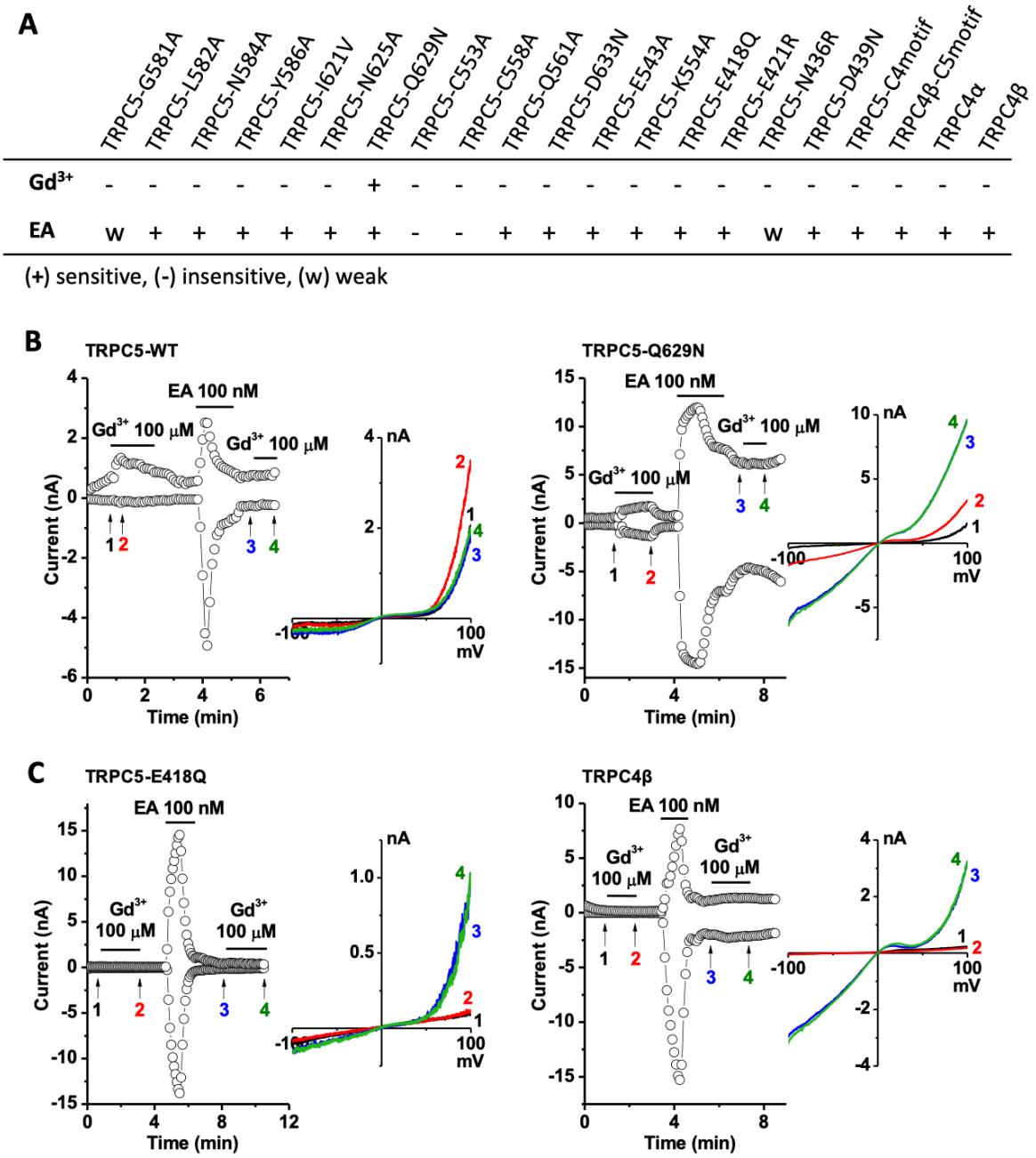

Fig. S6. Gd^{3+} potentiation is dependent on the unliganded and partially open state of TRPC5. (A) Sensitivity of TRPC5 and TRPC4 constructs to Gd^{3+} and EA. **(B-C)** Whole-cell patch clamp recordings of TRPC5 and TRPC4 constructs in response to Gd^{3+} and EA. The time course of currents measured at +80 and -80 mV and *I-V* relationships at arrow-indicated points are shown.

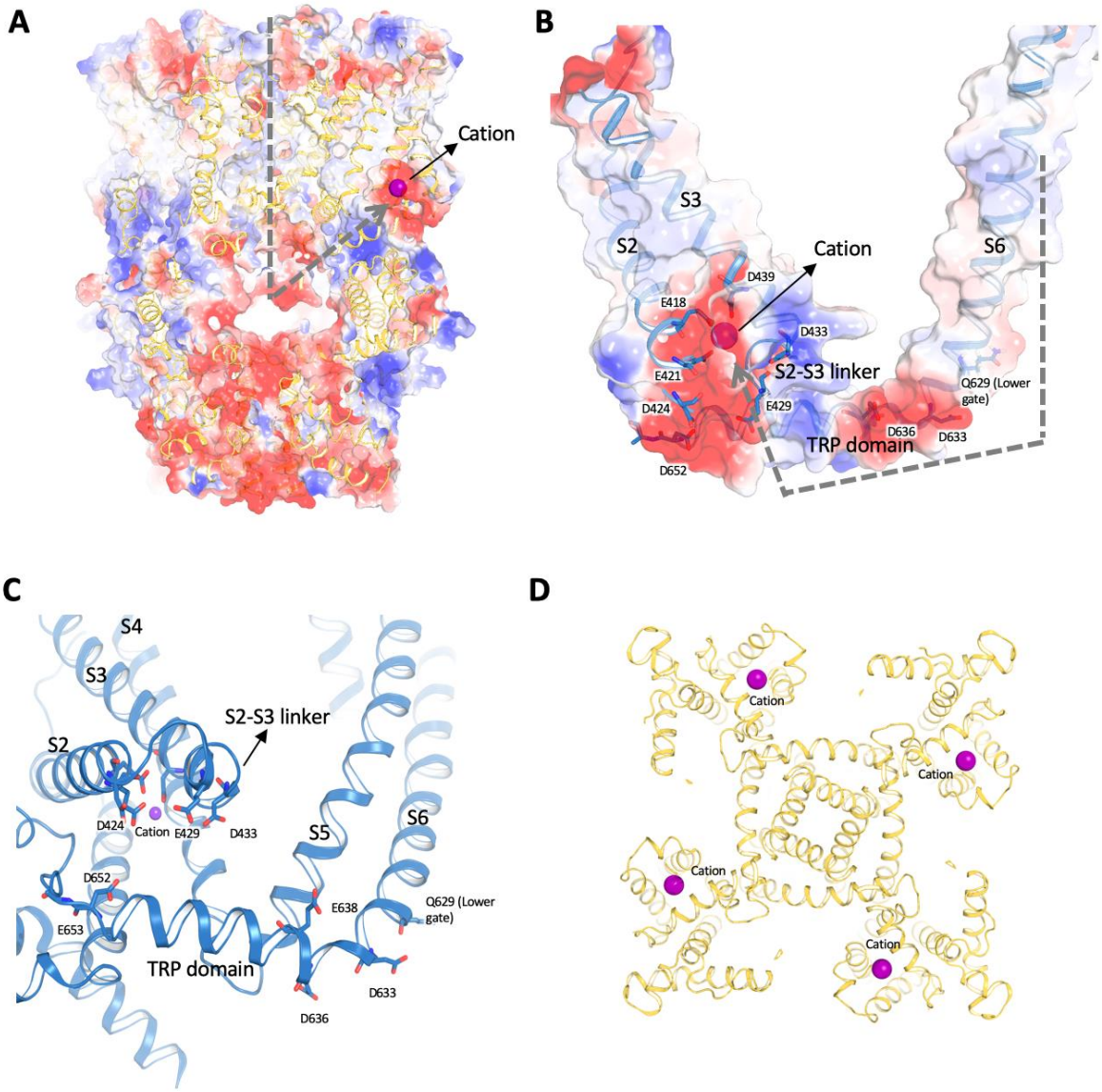

Fig. S7. The cation binding sites. Side and top views of electrostatic maps of cation binding pockets (not in the conduction pathway) in TRPC4; **(A)** tetramer and **(B)** monomer. Gray dots highlight possible pathways for cation entry. The surface is colored according to the calculated electrostatic potential, revealing the tetrameric distribution of charge. Blue indicates positive potential, red negative potential, and transparent white, neutral potential. **(C)** A number of negatively charged residues, including Asp633, Asp636, Glu638, Asp652 and Glu653 on the TRP domain, as well as Asp424, Glu429 and Asp433 on the S2-S3 linker, are aligned along the cation entry pathway. **(D)** The bottom view of the internal cation cavity.

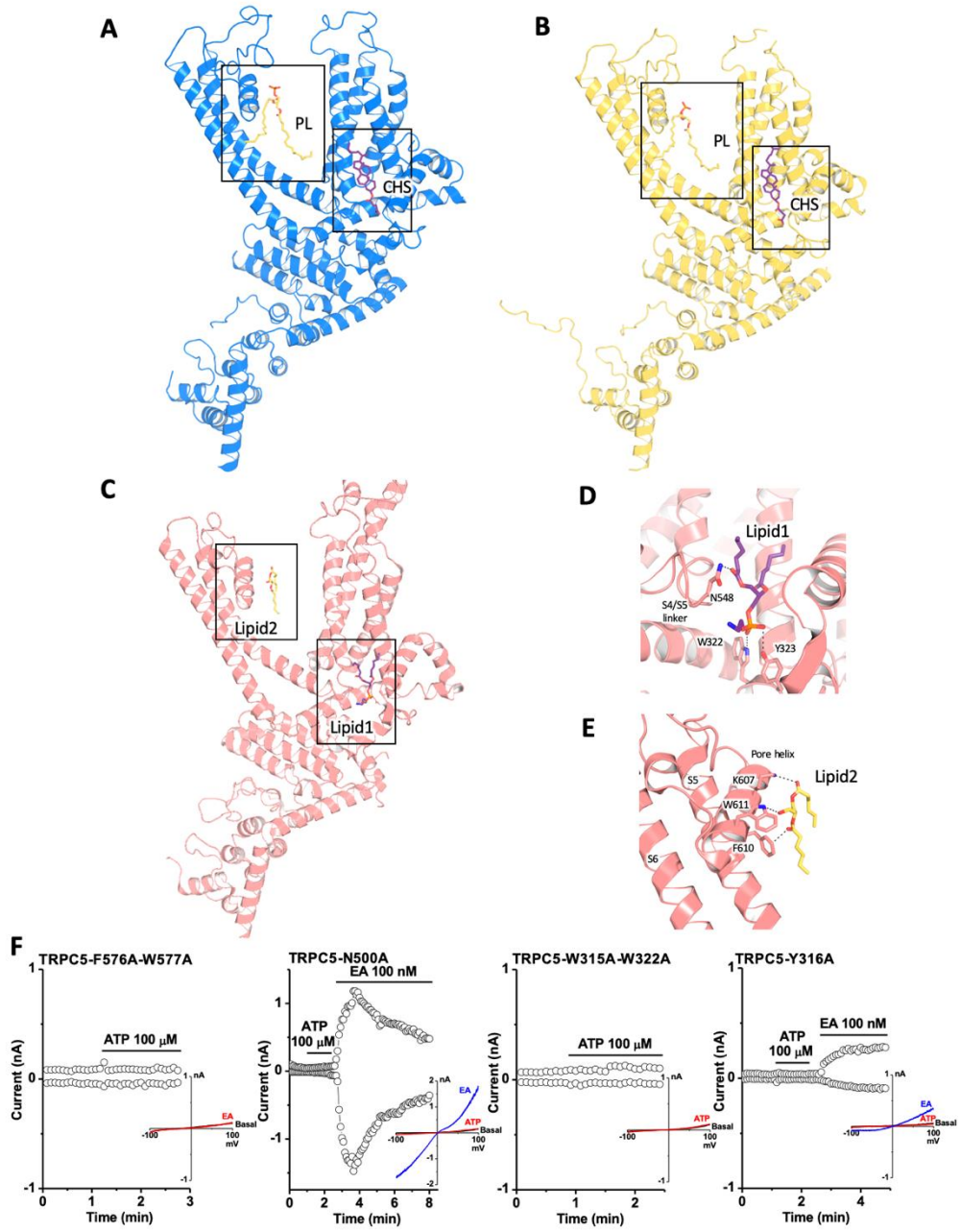

Fig. S8. Lipid-channel interactions. (A) Side view of the TRPC5 monomer. **(B)** Side view of the TRPC4 monomer. CHS (purple) and PL (yellow) molecules are shown as sticks. **(C)** Side view of TRPC3 monomer. Lipid1 (purple) and lipid2 (yellow) molecules are shown as sticks. **(D)** Lipid1 interacts with the S4/S5 linker at Asn548 and the N-terminal domains at Trp322 and Tyr323. **(E)** Lipid2 interacts with the pore helix through Lys607, Phe610 and Trp611. **(F)** Lipid-binding site mutants were not activated by ATP-induced GPCR signaling.

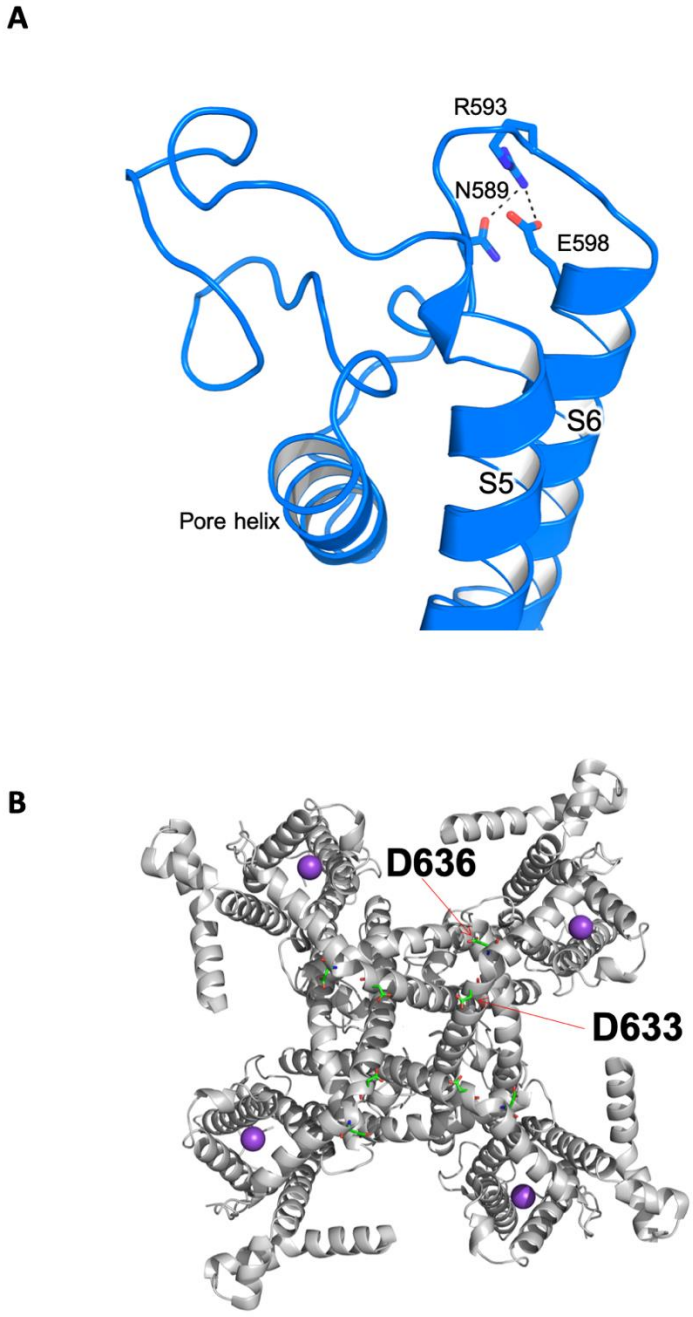

Fig. S9. Pore loop interactions and intracellular mouth of the channel pore. (A) Key residues located in the pore loop are shown in stick representation. Arg593 forms a hydrogen bond with Glu598. **(B)** Asp633 and Asp636 residues are shown in stick representation. Cation bound between S2 and S3 are shown as purple spheres. Carbon and oxygen atoms of residues are shown in green and red, respectively.

Table S1. Cryo-EM data collection, refinement, and validation statistics.

Cryo-EM of TRPC5	(EMD-9615) (PDB 6AEI)
Data collection and processing	
Microscope	FEI Tecnai Polara
Detector	Gatan K2
Calibrated magnification	40607
Voltage (kV)	300
Electron exposure (e–/Å^2)	42.3
Defocus range (μm)	0.6-3
Pixel size (Å)	1.23
Symmetry imposed	C4
Initial particle images (no.)	1164065
Final particle images (no.)	340465
FSC threshold	0.143
Map resolution (Å)	2.81
Map resolution range (Å)	2.5-4.0
Refinement	
Refinement software	phenix.real_space_refine
Initial model used (PDB code)	*de novo*
Model composition	
Non-hydrogen atoms	21157
Protein residues	2584
Ligands	13
B factors (Å^2)	
Average	62.6
R.m.s. deviations	
Bond lengths (Å)	0.007
Bond angles (°)	1.26
Validation	
MolProbity score	1.61
Clashscore	8.8
Ramachandran plot	
Favored (%)	98.25
Allowed (%)	1.75
Disallowed (%)	0